Encyclopedia of Computational Neuroscience
DOI 10.1007/978-1-4614-7320-6_333-1

Phototransduction Biophysics

Mikko Juusola[a]*, Zhuoyi Song[a] and Roger Hardie[b]
[a]Department of Biomedical Science, University of Sheffield, Sheffield, UK
[b]Department of Physiology, Development and Neuroscience, University of Cambridge, Cambridge, UK

Synonyms

Biophysical mechanisms that photoreceptors use to sample light information; Phototransduction cascade; Phototransduction mechanisms

Definition

Phototransduction biophysics comprises intracellular molecular reactions and ion fluxes through ion channels on the photoreceptor membrane that converts light into an electrical signal. Phototransduction biophysics serves the purpose of counting photons and integrating these counts to an estimate – a macroscopic voltage response – of light changes from a small area of visual space. To do this task well in vastly varying light conditions, photoreceptors rely upon stochastic adaptive sampling of light information.

Detailed Description

Basic Structure of Photoreceptor Cells

Photoreceptor cells of most animals are highly polarized, consisting of light-sensitive and light-insensitive parts (Fig. 1). The light-sensitive part is derived either from cilia or microvilli (Fain et al. 2010), forming a specialized light guide, such as the vertebrate rod/cone outer segment or fly photoreceptor rhabdomere, which facilitates directional photon capture along its longitudinal axis. Membrane elaborations – discs in rods or microvilli in fly photoreceptors – are enriched with the visual pigment protein rhodopsin. This absorbs light and activates a G-protein-based transduction cascade, bringing about the opening or closing of ion channels. Conversely, a photoreceptor's light-insensitive parts, which in vertebrate rods/cones form the inner segment, contain the cell body, axon, and synaptic machinery to transmit the resulting electrical signals to the retina network.

Microvilli Are Sampling Units

In a photoreceptor of the fruit fly (*Drosophila melanogaster*), each of its ~30,000 microvilli can be considered to be a photon counting or sampling unit (Fig. 2). Within a microvillus, following absorption of one photon by a single rhodopsin molecule, the phototransduction cascade culminates in the opening of ~15 TRP/TRPL channels (transient receptor potential and TRP-like channels; Hardie and Postma 2008). The resulting influx of calcium, magnesium, and sodium ions generates a quantum bump (sample). Although the exact mechanism of how TRP/TRPL channels are gated is still unclear, most aspects of microvillar phototransduction are known in sufficient detail (Hardie and

*Email: m.juusola@sheffield.ac.uk

DOI 10.1007/978-1-4614-7320-6_333-1

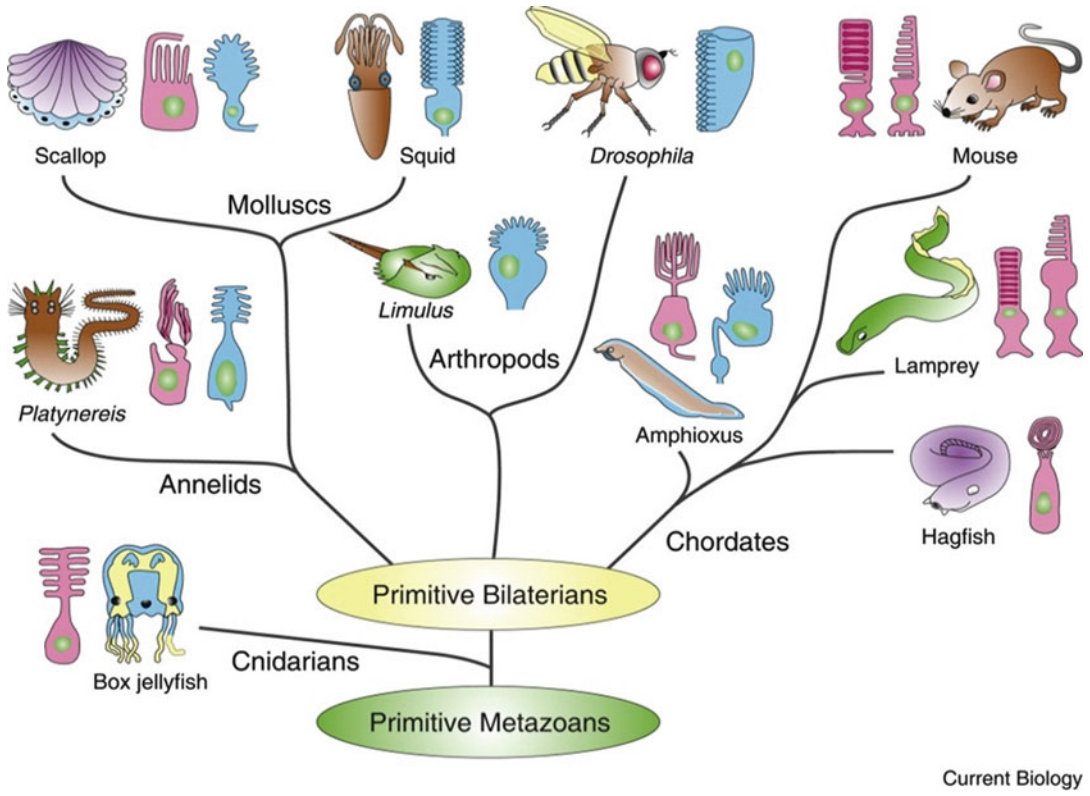

Fig. 1 *Ciliary and microvillar photoreceptors.* Photoreceptor types in principal eyes illustrated as ciliary (*red*) or microvillar (*blue*). Mammals and other vertebrates have ciliary photoreceptors (rods and cones) (From Fain et al. (2010))

Postma 2008; Hardie 2012; Hardie and Franze 2012) to allow the construction of molecularly explicit, stochastically operating computational models that accurately simulate the encoding of visual information (Song et al. 2012). The close correspondence between intracellular recordings and model simulations further suggests that vision benefits from stochasticity in phototransduction biophysics, with variable samples of microvilli summing up largely invariable responses to natural light patterns at different conditions (Faivre and Juusola 2008; Song et al. 2012).

Basic Rules of How a Photoreceptor Samples Light Information

A *Drosophila* photoreceptor is an imperfect photon counter that, nonetheless, produces highly reproducible macroscopic responses. Its responses to light stimuli can be largely predicted by these basic counting rules:

- A single microvillus (sampling unit) can produce only one bump (sample) at a time (Howard et al. 1987; Hochstrate and Hamdorf 1990; Pumir et al. 2008; Song et al. 2012).
- After producing a bump, a microvillus remains refractory (unavailable to sample) for up to hundreds of milliseconds; during this period, it fails to respond to other photons (Hochstrate and Hamdorf 1990; Scott et al. 1997; Mishra et al. 2007; Liu et al. 2008).
- Bumps from up to 30,000 microvilli integrate to yield the macroscopic response.
- Microvilli availability sets a photoreceptor's maximum sample rate (bump production rate), adapting its macroscopic response to a light stimulus (Howard et al. 1987).

DOI 10.1007/978-1-4614-7320-6_333-1

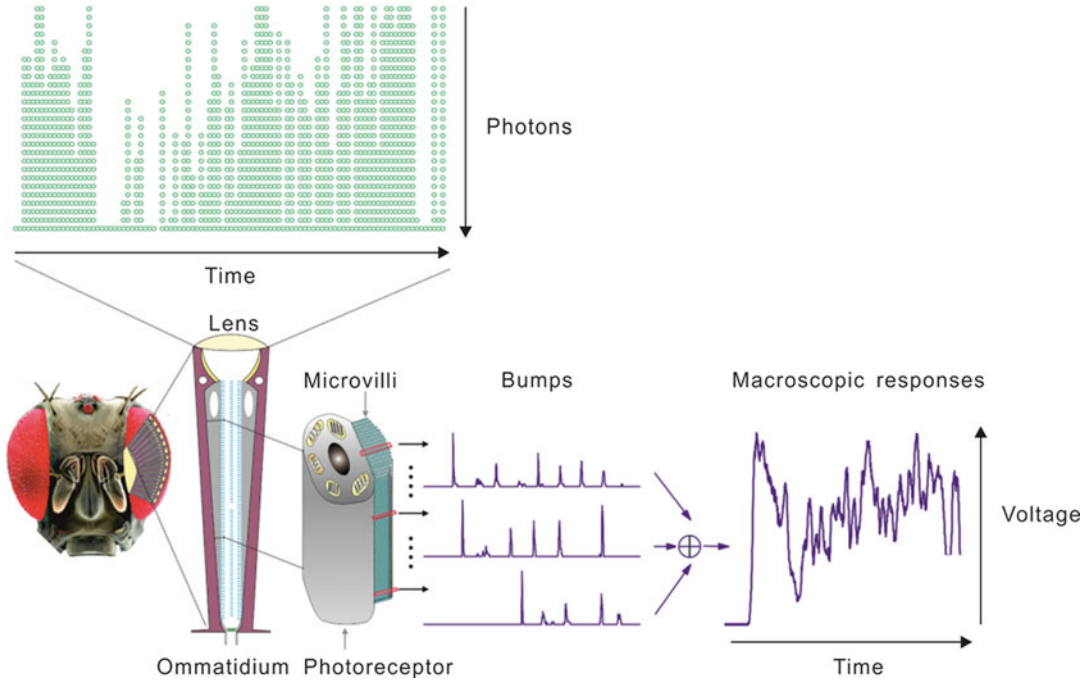

Fig. 2 *Stochastic adaptive sampling in a Drosophila photoreceptor.* Photons are sampled by a population of 30,000 microvilli, stacked layer by layer on one side of the photoreceptor soma, forming the light-guiding rhabdomere. In the microvilli, the rate, size, and speed of their photon-evoked elementary responses (bumps or samples) vary stochastically yet adapt continuously, integrating to a consistent (anti-aliased) macroscopic response

- Global calcium accumulation and membrane voltage affect samples of all microvilli. These global feedbacks strengthen with brightening light to reduce the size and duration of bumps, adapting the macroscopic response (Wong and Knight 1980; Wong et al. 1982; Juusola and Hardie 2001b).

Phototransduction Reactions: From Photon Absorption to a Bump

Phototransduction in *Drosophila* is a canonical G-protein-coupled phospholipase C-based cascade (Hardie and Postma 2008; Yau and Hardie 2009; Hardie 2012). Essential elements of the cascade including the channels are localized within a microvillus (Fig. 3), which together with its ~30,000 neighbors form the light-guiding rhabdomere.

As in all photoreceptors, the cascade is initiated by absorption of a photon by a chromophore (3-OH 11-*cis* retinaldehyde) covalently attached to rhodopsin (R). Photoisomerization of the 11-*cis* retinal to the all-trans configuration by a single photon converts R to the active metarhodopsin state (M), which catalytically activates a heterotrimeric Gq-protein releasing the active Gqα subunit. About 5–10 Gqα subunits are released by each activated M within the same microvillus during the brief but variable latency period, and diffuse in the plane of the membrane before binding to and activating a phospholipase C (PLC) molecule. Each of the 5–10 PLC molecules (Fig. 3) thus activated and then hydrolyzes the minor membrane phospholipid, PIP2, at a rate of ~1,000 molecules per second, causing a physical contraction of the microvillar membrane as well as yielding inositol triphosphate (InsP3), diacyl glycerol (DAG), and a proton.

Although still debated, the most recent evidence suggests that it is the combination of membrane contraction and proton release that then results in the gating of the Ca^{2+} permeable TRP (and TRPL) light-sensitive channels (Huang et al. 2010; Hardie and Franze 2012). Powerful positive feedback

DOI 10.1007/978-1-4614-7320-6_333-1

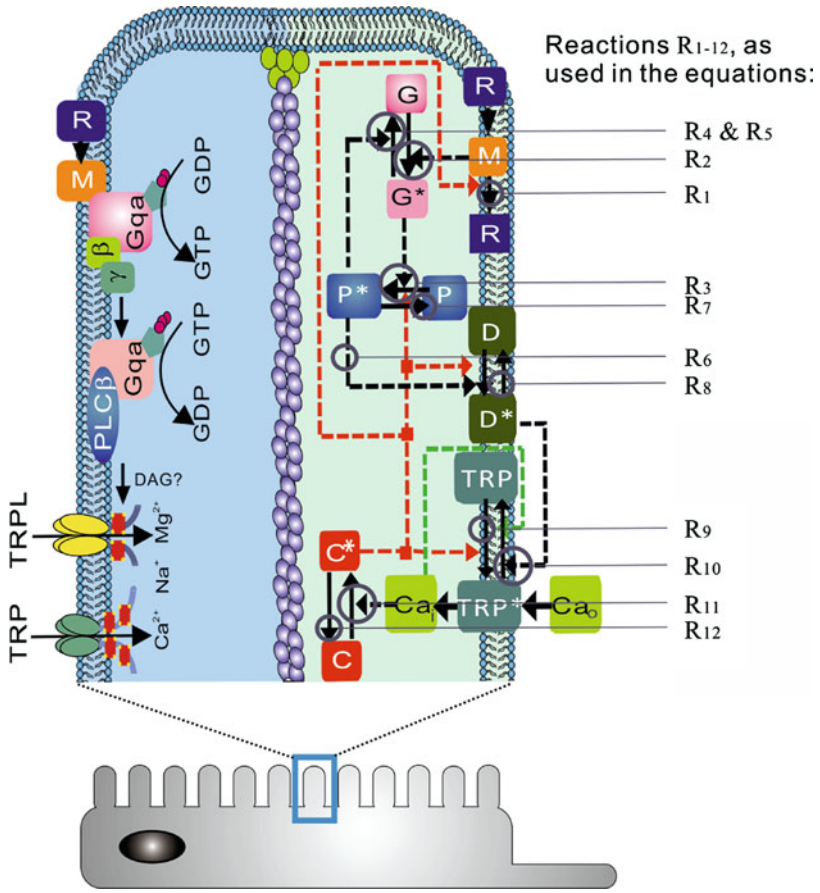

Fig. 3 *Each microvillus contains a full transduction cascade, which generates variable bumps or failures to absorbed photons. Left side*: molecular participants in microvillar phototransduction reactions. M^* metarhodopsin, C^* Ca^{2+}-dependent feedback, which acts as negative feedback to multiple targets, D^* DAG, P^* G-protein-PLC complex. *Right side*: the corresponding reactions, R1–R12 (indicated by *black arrows*), as used in the stochastic model (see Eqs. below) and in Fig. 4a. *Red dotted arrows* indicate negative feedbacks; *green dotted line*, positive feedbacks. In this schematic, DAG? stands for the yet unresolved gating mechanism that includes production of DAG, InsP3, proton, and physical microvilli contraction (Adapted from Song et al. (2012))

mediated by Ca^{2+} influx via the first activated TRP channel rapidly facilitates activation of the remaining channels in the microvillus. This floods the microvillus with up to ~1 mM Ca^{2+}, rapidly terminating the response by Ca^{2+}-dependent negative feedback at multiple targets including the channels themselves. The final electrical response to a single effectively absorbed photon is a ~10 pA quantum bump (Fig. 4a), representing the opening of most of the ~20 TRP channels in a single microvillus.

The macroscopic light-induced current (LIC) represents the summation of the quantum bumps of variable sizes (Fig. 4b) and timings (Fig. 4c), independently generated over the 30,000 microvilli.

Why Some Absorbed Photons Fail to Be Counted?

In a microvillus, the likelihood, size, and timing of a new bump depend upon the success, stochasticity, and finite speed of phototransduction reactions, all partly affected by the history of past bumps in the same microvillus and global Ca^{2+} levels integrated from bumps across the whole cell (Fig. 4a). In darkness, virtually every absorbed photon causes a bump (nearly 100 % quantum efficiency), but with brightening illumination, the quantum efficiency of a microvillus decreases.

DOI 10.1007/978-1-4614-7320-6_333-1

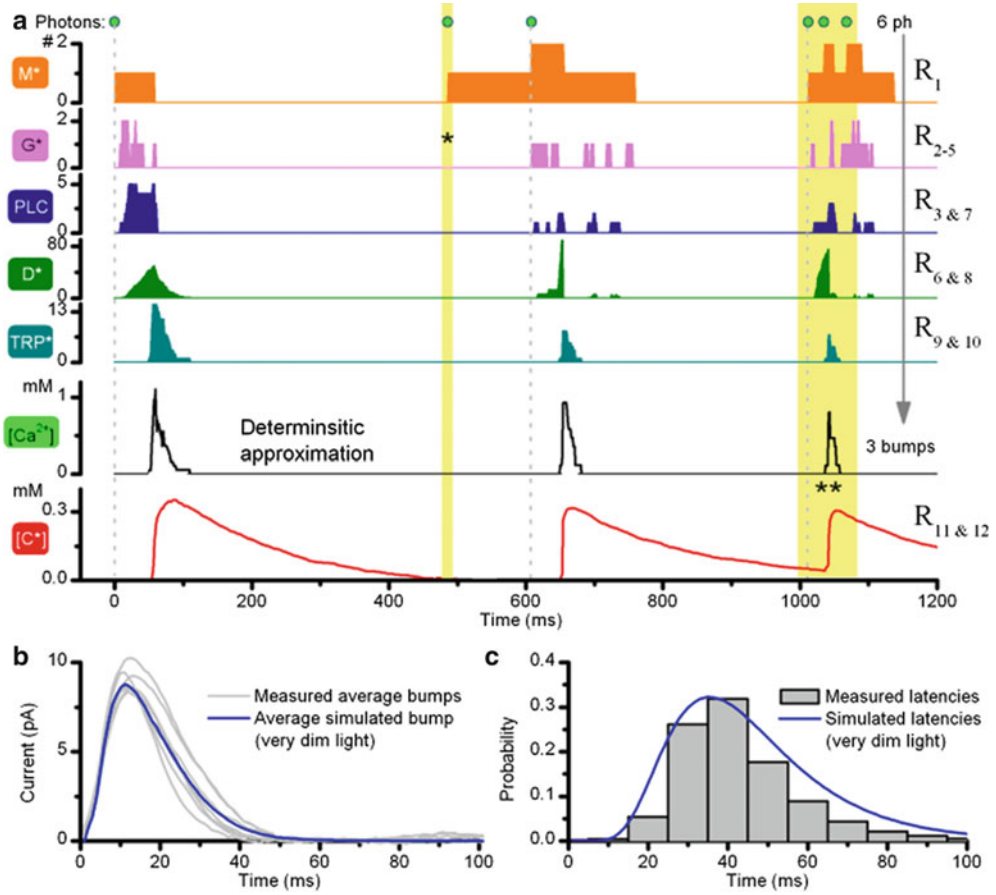

Fig. 4 *Reactions inside a microvillus are modeled in a stochastic framework, with known molecular interactions, using physiologically measured parameters.* (**a**) Simulations show how a microvillus generates elementary responses (bumps) to captured photons; after a "dead time," 5–15 TRP channels open, mediating Ca^{2+} and Na^{+} influx into the microvillus. Ca^{2+}-dependent feedback (*red*) provides negative feedback, which prevents new bumps until the feedback is low. * = G^{*} activation failed; ** = negative feedback blocked two photon activations. $[C^{*}]_i$ decay phase is longer than the real refractory period, which represents a balance between the feedbacks; the positive feedback can outgrow the negative one in the middle of $[C^{*}]_i$ decay. Thus, a bump can be generated without C^{*} being zero (e.g., the third bump). (**b**) Average recorded and simulated bumps are similar. The bump current is given by Eq. 1. (**c**) Latency distributions of simulated and real bumps are similar (Adapted from Song et al. 2012)

Rarely, the cascade molecules may fail to activate their upstream targets and the signal dies. More often, the reactions stop prematurely because the photons arrived before the refractory period (50–200 ms) of the last bump had faded. Here, intra-microvillar calcium provides sequential positive and negative feedbacks to multiple targets, amplifying the signal and accelerating response speed (Hardie and Postma 2008).

Biophysical models (Pumir et al. 2008; Song et al. 2012) indicate that as soon as a bump is generated, the negative feedback holds the microvillus in a state of inhibition during which it cannot respond to light. This refractory period represents a balance between the positive and negative feedbacks. It ends when the positive feedbacks outgrow the relaxing negative feedbacks and ultimately set the maximum sample rate (bump production rate) of the microvillus (Hochstrate and Hamdorf 1990; Scott et al. 1997; Mishra et al. 2007; Liu et al. 2008).

DOI 10.1007/978-1-4614-7320-6_333-1

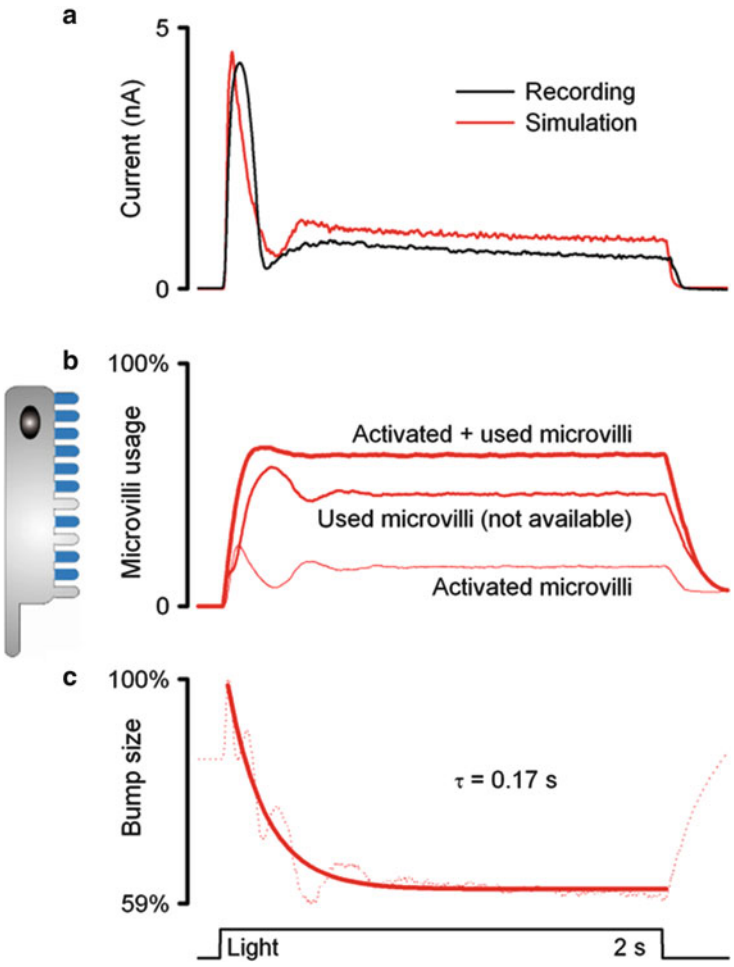

Fig. 5 *Availability of microvilli and their adapting bumps shape responses to light.* (**a**) LIC to a bright pulse recorded from dissociated R1–R6 *Drosophila* photoreceptors (R1-R6 are the six outer photoreceptors in a single ommatidium) during whole-cell patch clamp (*black*) and a simulated LIC (*red*) to the same stimuli. LIC is shaped by the number of activated microvilli (**b**) and negative feedback, which reduces the size of the bumps they produce (**c**). (**b**) Output of 30,000 microvilli modeled, showing the fractions of used (refractory) and activated microvilli and their sums in the model simulations to reproduce (**a**). (**c**) *Dotted line* shows the ratio of the normalized LIC (**a**) and the number of activated microvilli (**b**), which represents the effect of a reduction in bump waveform on LIC as a function of time (whereas the refractory period affects microvilli usage). Bump size begins to diminish already after the first bumps, which shape the initial transient response. Time course of bump adaptation is approximated by a single exponential. In (**a**), most differences between the traces are due to a fixed (*light* adapted) refractory period distribution, which was used in the simulation

How Changes in Sampling Result in Adapting Macroscopic Responses?

Adaptation in macroscopic response (Fig. 5a) to continuous light is mostly caused by reduction in the (i) number and (ii) size of samples over time.

(i) At the stimulus onset, a large fraction of the microvilli is activated simultaneously but then becomes refractory (Fig. 5b). This leaves a smaller fraction of the microvilli to respond to the next photons in the stimulus until more microvilli become available again. Therefore, the number of activated microvilli (samples) first peaks, followed by a rapid drop before settling to a steady state as photon arrivals and refractory periods balance.

(ii) If all bumps were identical, then the macroscopic current would simply represent the number of activated microvilli at a given photon rate, with a flattened steady-state response. However, real light-induced currents show decaying trends toward lower plateau levels. This is because bumps adapt (Fig. 5c), becoming smaller and briefer with brighter backgrounds (Wong and Knight 1980; Wong et al. 1980, 1982; Juusola and Hardie 2001b). This global negative feedback likely stems from Ca^{2+}-dependent inhibition due to light-induced calcium spread between microvilli via the cell body (Hardie 1996; Postma et al. 1999; Hardie and Postma 2008). This attenuates bump waveforms by progressively strengthening the negative feedback to multiple targets. Furthermore, the resulting membrane voltage increase also compresses responses by reducing the electromotive force for the light-induced current across all microvilli (Song et al. 2012).

Thus, experiments and simulations suggest that reduction both in the number of samples (activated microvilli) and in their size (bump waveforms) largely accounts for adaptation in the macroscopic response.

What Governs the Rate of Information Transfer of Macroscopic Responses?

The signal-to-noise ratio and rate of information transfer increase with the average sampling rate, which is the average number of samples per unit time. Thus, the more samples that make up the macroscopic response to a given light pattern, the higher is its rate of information transfer (Fig. 6). However, with more photons being counted by a photoreceptor at brightening stimulation, information about naturalistic light patterns in its responses first increases and then approaches a constant rate. This is because:

(i) When more microvilli are in refractory state, more photons fail to generate bumps. As quantum efficiency drops, the equilibrium between used and available microvilli approaches a constant (maximum) bump production rate (sample rate).
(ii) Once global calcium and voltage feedbacks saturate, they cannot make bumps any smaller and briefer with increasing brightness.
(iii) After initial acceleration from the dark-adapted state, bump latency distribution remains practically invariable in different light-adaptation states (Juusola and Hardie 2001b).

Therefore, when sample rate modulation (i) and sample integration dynamics (ii and iii) of the macroscopic voltage responses settle (at intensities $>10^5$ photons/s in *Drosophila* R1–R6 photoreceptors; Fig. 6a–d), allocation of visual information in the photoreceptor's amplitude and frequency range becomes nearly invariable (Faivre and Juusola 2008; Song et al. 2012). Correspondingly, stochastic simulation closely predicts measured responses and rates of information transfer (Zheng et al. 2006, 2009; Gonzalez-Bellido et al. 2011; Song et al. 2012). Notably, when the microvilli usage reaches a midpoint (~50 % level) (Fig. 6e), the information rate encoded by the macroscopic responses to natural light intensity time series saturates (Song et al. 2012). This is presumably because sample rate modulation to light increments and decrements – which in the macroscopic response code for the number of different stimulus patterns (Juusola and de Polavieja 2003) – saturate.

Bump size, if invariable, does not affect the rate of information transfer – as long as the bumps are briefer than the stimulus changes they encode. Thus, like any other filter, a fixed bump waveform

DOI 10.1007/978-1-4614-7320-6_333-1

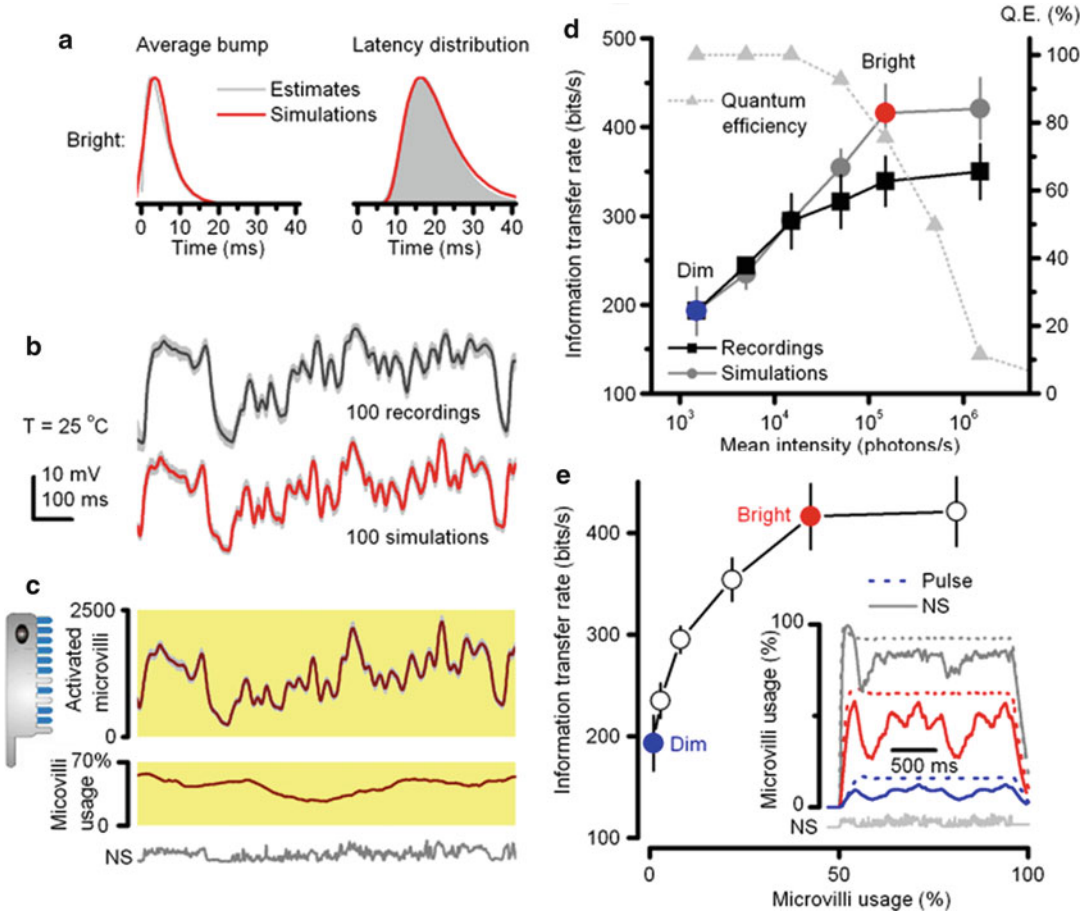

Fig. 6 *In a fully light-adapted state, sample (bump) rate changes define the rate of information transfer of macroscopic responses.* (**a**) Stochastic microvilli models can be set to use the corresponding average bump waveforms and latency distributions, estimated from the white-noise contrast experiments at different light levels, by refixing two model parameters: n_s (Eq. 7) for the bump shape and *la* (Eq. 8) for the latency distribution. (**b**) 100 superimposed responses (*light gray*) and the average signal to a repeated bright naturalistic stimulus (NS), and the corresponding simulations. (**c**) The NS activates microvilli stochastically with appropriate dynamics and statistics. Owing to largely low-frequency input (1/f statistics), the number of activated microvilli is mostly responsible for the corresponding response waveforms (**b**). This encoding uses only a fraction of 30,000 microvilli (maximally ∼ 68 % for the repeated NS) because the NS contains long relatively dim periods, allowing refractory microvilli to return to the pool of available ones during stimulation. (**d**) Information transfer rate of photoreceptors (*black*) and the model (*gray*) to the same NS at six different light levels. Recordings' lower information transfer at three brightest intensities can be attributed to damage, experimental noise, and intracellular pupil, which progressively filter out photons. At dim intensities, the effect of experimental noise and adaptation may be compensated by the synaptic network introducing new information from neighboring photoreceptors. Quantum efficiency (QE) of simulated photoreceptor output drops with brightening of the NS, while the information transfer approaches a constant rate. (**e**) Information transfer reaches maximum when about 50 % of microvilli are in continuous use and is maintained, despite steep falloff in quantum efficiency (QE) at the brightest intensities (**d**). Inset: during a very bright NS, because of its 1/*f* statistics that contain interspersed darker periods, proportionally more microvilli recover than during light pulses (*dotted lines*) of equal mean intensity. A very bright pulse (10^6 photon/s) activates ∼ 99 % of microvilli at the beginning of stimulation, and their usage remains high throughout the pulse. Error bars show SD (Adapted from Song et al. 2012)

affects signal and noise equally (data processing theorem; Shannon 1948; Juusola and de Polavieja 2003; Song et al. 2012). But varying bump size adds noise; when this variation is adaptive (memory based), less noise is added (Song et al. 2012).

What Are the Coding Benefits of Global Feedbacks?

In bright light, global calcium and voltage feedbacks reduce bump amplitudes and durations, enabling more evenly encoded macroscopic responses that can utilize a smaller voltage range. This likely reduces a photoreceptor's energy consumption (Laughlin et al. 1998).

Together with the stochastic latency and refractory period distributions, the bump waveform regulates the size (gain) and speed (frequency range) of macroscopic responses (Juusola and Hardie 2001b; Faivre and Juusola 2008; Song et al. 2012). In very dim conditions, quantum efficiency is near 100 % and the influence of global feedbacks is minimal. This leads to generation of large variable bumps with broad timing jitter, integrating macroscopic responses of high sensitivity. In bright conditions, conversely, quantum efficiency is <1 % and global feedbacks are maximal. The outcome is smaller, less variable, and better synchronized bumps, which integrate to a macroscopic response of lower sensitivity. However, in large part due to the low-frequency dominated spectra of natural images (1/f), the macroscopic response waveforms to dim or bright natural light intensity time series are very similar (Faivre and Juusola 2008; Song et al. 2012).

In diurnal insect photoreceptors that have been tested both in dark- and light-adapted conditions (Juusola and Weckstrom 1993; Juusola and Hardie 2001a, b; Faivre and Juusola 2008; Gonzalez-Bellido et al. 2011), the bandwidths of their membranes show higher cutoff frequencies than those of their light-induced currents. Thus, the global voltage feedback compresses – by reducing the electromotive drive of light-induced current (Song et al. 2012) – the responses without much influencing the frequency allocation of the transmitted information (Shannon 1948; Juusola and de Polavieja 2003).

In summary, global feedbacks perform important energy-efficient normalization processes. These enable variable samples and counts to add up to similarly shaped macroscopic voltage responses for natural light changes in different illumination conditions, paving the way for perceptually invariant neural representations of visual objects.

What Are the Benefits and Costs of Adaptive Stochastic Sampling?

Stochastic sampling is not only an elegant light-adaptation strategy but may also represent a novel, generic solution to the temporal aliasing problem. It scatters high-frequency information into broadband noise rather than generating the false patterns produced by regular sampling (Leneman 1966). Thus, variable sampling times and sample sizes prevent distortions or artifacts in reconstruction of macroscopic responses from the original (continuous) light patterns. Similarly, topological disorder of photoreceptors in retinae likely provides anti-aliased sampling of spatial (Yellott 1982) and chromatic (Wardill et al. 2012) information from visual scenes. Intrinsic biophysical heterogeneity in neuron populations can further increase information content and robustness of their collective spatiotemporal signal (Heimonen et al. 2006; Padmanabhan and Urban 2010).

The trade-off of stochastic sampling is broadband noise (Leneman 1966; Dippe and Wold 1985). However, in fly photoreceptors – due to global feedbacks that carry memory of the past events – such noise is reduced by adapting the sample sizes to the ongoing light stimulation. This accounts for about 10 % improvement in the rate of information transfer, in comparison to sampling the bumps randomly from the same distribution (Song et al. 2012). Noise is further reduced when signals from neurons converge, e.g., when macroscopic responses of photoreceptors, which sample light from the same point, are pooled in synaptic transmission to interneurons (Zheng et al. 2006).

Specifically in fly photoreceptors, adaptive stochastic sampling has been shown to (Song et al. 2012):

DOI 10.1007/978-1-4614-7320-6_333-1

- Resist saturation – It is hard to knock out all microvilli at once, as there are always some returning to the pool of available ones in any one moment.
- Improve the signal-to-noise ratio of macroscopic responses, in comparison to corresponding estimates that are sampled randomly (without memory) from the same bump waveform distribution.
- Reduce oscillations in macroscopic responses to sudden stimulus changes.
- Utilize microvilli and the amplitude range of photoreceptor output more evenly. Notably, a macroscopic response, in which every voltage level is utilized equally often, would have the highest information content (Shannon 1948; Zheng et al. 2009).
- Promote equalizing of contrast information transfer in different light conditions.
- Evoke similarly shaped responses in different light conditions.
- Enhance responses to novel stimuli (Juusola and de Polavieja 2003). Events which generate the largest changes in microvilli activation (sample rate modulation bump increments or decrements) with respect to the ongoing average are represented by macroscopic responses with the highest information content (Song et al. 2012).

Photoreceptor Structure Defines Its Encoding Performance

Models of different fly photoreceptors indicate that their structures and biophysical makeup are intrinsically linked to the neural signaling they carry out (Song et al. 2012). Thus, differently shaped photoreceptors of different species presumably evolved to match the visual requirements of their lifestyle. A photoreceptor's maximum information transfer rate cannot be increased beyond its structural limits, hardwired in the maximum number microvilli and in their maximum bump production rate (Fig. 7). Photoreceptors with the most and fastest microvilli in principle provide the best vision. However, this comes at a price: more microvilli increase plasma membrane's capacitance and potentially its time constant. The larger (slower) time constant can only be offset by larger conductances, ultimately consuming more ATP (Laughlin et al. 1998; Fain et al. 2010).

Appealing analogy: Sir Francis Galton realized that the mean of variable samples, reported independently by honest observers, provides the best estimate of the witnessed event (Galton 1907). In fly photoreceptors, the observers are the tens of thousands of microvilli. Each of them has either encountered photons recently or not. A microvillus that absorbs a photon casts an independent vote on how important (surprising) that event is, given the past light history. Accordingly, the weighted average of all the sampled simultaneous votes (macroscopic response) provides a reliable (non-aliased) neural estimate of the ongoing light signal. This information matches the visual requirements of the animal, as embedded in its hardwired photoreceptor structures and stochastic phototransduction biophysics (Gonzalez-Bellido et al. 2011; Song et al. 2012).

Biophysical Photoreceptor Model

A biophysical model of a *Drosophila* photoreceptor that can generate realistic responses to time series of light intensities contains four modules (Song et al. 2012):

(i) Random Photon Absorption Model: regulates photon absorptions in each microvillus, following Poisson statistics.
(ii) Stochastic Bump Model: stochastic biochemical reactions inside a microvillus capture and transduce the energy of photons to variable bumps or failures.
(iii) Summation Model: bumps from 30,000 microvilli integrate to the macroscopic light-induced current (LIC) response.

DOI 10.1007/978-1-4614-7320-6_333-1

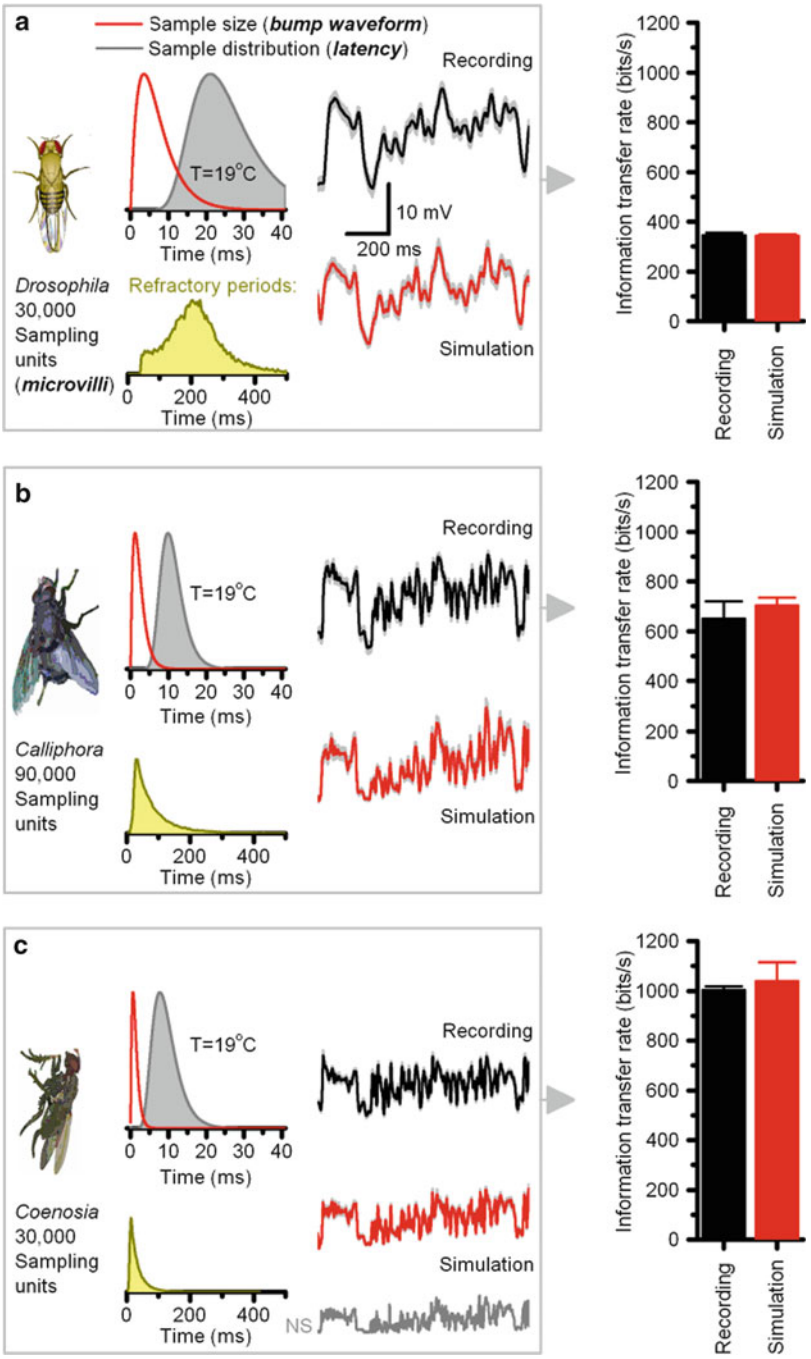

Fig. 7 *Photoreceptor models of adaptive sampling behave like real photoreceptors.* (**a**–**c**) Outputs of *Drosophila*, *Calliphora,* and *Coenosia* photoreceptors, respectively, were simulated by stochastic models. The microvilli numbers were fixed to match those of the real cells, and their average bump waveforms (*dark red*) and latency distributions (*gray*) were approximated from in vivo recordings by adjusting the negative feedback strength within their microvilli, by refixing two global negative feedback parameters: n_s and *la*. These photoreceptor models' voltage responses (*red*) to the repeated presentations of a naturalistic stimulus (NS) pattern behave as their real counterparts (*black*). Lower insets show the corresponding refractory periods (inter-bump intervals, *yellow*), generated by the microvilli of the models to the NS. Information transfer rates (*right*) of the simulated responses follow those of the real recordings (Adapted from Song et al. 2012)

DOI 10.1007/978-1-4614-7320-6_333-1

(iv) Hodgkin-Huxley (HH) Model of the photoreceptor plasma membrane: transduces LIC into a voltage response.

This modeling approach is robust and does not require full knowledge of all molecular players and dynamics in the phototransduction process. From a computational viewpoint, the exactness of the simulated molecular interactions is not important. As long as the photoreceptor model contains the right number of microvilli, each of which is a semiautonomous sampling unit, and their stochastic bump dynamics (average waveforms, latency distribution, and refractory period) approximate those in the real recordings, it will sample and process information much like a real photoreceptor (Song et al. 2012).

Random Photon Absorption Model

- Input: the number of photons absorbed by the rhabdomere in each 1 ms time interval
- Output: the number of photons absorbed by each microvillus

With photon absorptions following Poisson statistics (Hochstrate and Hamdorf 1990), variable numbers of photons are absorbed by each microvillus in the rhabdomere. Because the bump/photon ratio in each microvillus changes with the number of photons it absorbs, this model is needed for generating a realistic light input for each microvillus.

Key assumptions:

- Each microvillus absorbs photons independently with all microvilli having the same absorption probability. These assumptions eliminate the role of rhabdomere topology, simplifying calculations. In rhabdomeres, microvilli taper, with their photon absorption probabilities at the bottom being likely less than those at the top. Nonetheless, because simulations pair well with the experimental results, probabilistic scaling of the photon flux (through the tapering microvilli) is not critical.

As there are ~30,000 microvilli in a *Drosophila* photoreceptor rhabdomere, if the light input contains N_{ph} photons in the given time interval (1 ms), the average number of photons a single microvillus can absorb is $\lambda_M = N_{ph}/30{,}000$. Following Poisson statistics, the fraction of microvilli that absorb k photons is $p(k) = \lambda_M^k e^{-\lambda_M}/k!$. Therefore, $30{,}000 \times p(k)$ microvilli can be uniformly drawn to absorb k photons at one time point, where $k < k_n$; k_n is the smallest number that satisfies $p(k_n) < 1/30{,}000$. This procedure iterates along the light time series with each microvillus obtaining an absorbed photon series to stimulate its phototransduction cascade.

Stochastic Bump Model

- Input: the number of photons absorbed by each microvillus
- Output: variable bumps generated by each microvillus

Stochastic phototransduction cascade models simulate known enzymatic reactions (Pumir et al. 2008; Song et al. 2012), generating variable bumps (samples) to absorbed photons. Bump series to sequential photon absorptions are needed for investigating continuous adaptation processes. Despite the many model parameters, adaptation can be regulated by two master parameters: n_s in Eq. 7 for bump shape and *la* in Eq. 8 for bump latency distribution. The model also includes a representation of $[Ca^{2+}]$ dynamics.

DOI 10.1007/978-1-4614-7320-6_333-1

To account for the intrinsic variability in the reactions, where several molecular interactions occur at low numbers, the quantum bump model uses a stochastic simulation framework based on the Gillespie algorithm (Gillespie 1976).

Key assumptions:

- Because spontaneous bumps are very rare (Hardie and Postma 2008), reactions are assumed to be silent in the dark-adapted state.
- A well-mixed chemical system is assumed for simplicity. All the reaction pathways are decomposed into M unidirectional elementary reaction steps R_μ. Each of these reaction steps is characterized by a momentarily defined stochastic reaction constant, c_μ, where $c_\mu \delta t$ ($\mu = 1, 2, \ldots, M$) denotes the average probability that a particular combination of R_μ reactant molecules will react accordingly in the next infinitesimal time interval δt.

If h_μ is the total number of R_μ reactant pairs, then $a_\mu \delta t = c_\mu h_\mu \delta t$ is the average probability that reaction R_μ will occur during δt. By considering a discrete infinitesimal time interval, (t, $t + dt$), during which 0 or 1 reaction occurs, dt and R_μ can be determined independently. When R_μ is chosen, the state vector $\mathbf{X}$ is updated with a state transition vector, $\mathbf{V}_\mu$. The procedure iterates until a termination criterion is satisfied, e.g., if the current simulation time, t, is larger than a preset value.

The molecules are counted when there are only a few in each microvillus. Otherwise, concentrations are used, calculated using the microvillus volume. In the equations or reactions, X is the number of molecules; X^* is the active state of X, and X_T the total number of corresponding molecules/channels inside a single microvillus. $[X]$ is the concentration; $[X]_i$ is intracellular concentration and $[X]_o$ the extracellular concentration. Rates of activation are denoted by κ and rates of deactivation by γ. Positive and negative feedbacks are f_p and f_n, respectively, and the local feedback strength parameter is h.

The signaling pathway is decomposed into a set of unidirectional reactions, R1–R12 (indicated by arrows in Fig. 3, right side), each of which contains only unimolecular or bimolecular reactants:

$$M^* \xrightarrow{c1} \phi \tag{R1}$$

$$M^* + G \xrightarrow{c2} M^* + G^* \tag{R2}$$

$$G^* + PLC \xrightarrow{c3} PLC^* \tag{R3}$$

$$G^* + PLC^* \xrightarrow{c4} G_\alpha GDP + PLC^* \tag{R4}$$

$$G_\alpha GDP \xrightarrow{c5} G \tag{R5}$$

$$PLC^* \xrightarrow{c6} D^* + PLC^* \tag{R6}$$

$$PLC^* \xrightarrow{c7} PLC + G_\alpha GDP \tag{R7}$$

DOI 10.1007/978-1-4614-7320-6_333-1

$$D^* \xrightarrow{c8} \phi \tag{R8}$$

$$2D^* + T \xrightarrow{c9} T^* \tag{R9}$$

$$T^* \xrightarrow{c10} T \tag{R10}$$

$$\mathrm{Ca}^{2+} + CaM \xrightarrow{c11} C^* \tag{R11}$$

$$C^* \xrightarrow{c12} \mathrm{Ca}^{2+} + CaM \tag{R12}$$

Because the input is the number of absorbed photons, photon-activated rhodopsin (metarhodopsin, M^*) is incremented by 1 if one photon is absorbed in a microvillus.

In the unidirectional reactions:

- R1 is the inactivation of metarhodopsin (M^*) by arrestin binding; ϕ indicates any reaction product, whose kinetics is not modeled. G-proteins can exist in multiple states. For simplicity, only the cycle through three states is modeled: $G_\alpha G_{\beta\gamma} GDP$ (G), $G_\alpha GTP$ (G^*), and $G_\alpha GTP{-}PLC$ (PLC^*).
- R2 is the activation of G into G^* by M^*.
- In R3, G^* binds to PLC and becomes an active G-protein-PLC complex (PLC^*).
- R4 and R5 represent the recycling process of G-proteins. R4 is the conversion from $G_\alpha GTP$ to $G_\alpha GDP$ by GTPase activity of G^*, supposedly catalyzed by PLC^*. $G_\alpha GDP$ then rebinds to $G_{\beta\gamma}$ before it can be reactivated (R5).
- PLC^* hydrolyzes PIP_2 into DAG and IP_3, generating the unknown excitation messengers for TRP/TRPL channels. In R6, because of this ambiguity, PLC^* is modeled to activate the supposed excitation messenger D^* directly.
- D^* excites TRP/TRPL channels T to their open states (T^*) in R9 and is degraded in R8.
- R10 is the process of closing the open TRP/TRPL channels.
- R11 is the binding of Ca^{2+}, which enters the microvillus through the open TRP/TRPL channels, to Calmodulin C^*. R11 is a simplified first-order representation of the Ca^{2+} binding process, where in reality, 4 calcium ions bind to CaM to form C^*.
- R12 is the release of Ca^{2+} from Calmodulin.
- Ca^{2+}-bound Calmodulin constitutes the feedback intermediate for regulating the reactions R1–R10.

In these reactions and under voltage-clamped conditions, the light-induced current, I_{in}, is the product of T^* (the output for the phototransduction cascade) and I_{T^*} (the average single-channel current conducted by an open TRP/TRPL channel).

Assuming that, apart from Ca^{2+}, the molecular components cannot enter or leave the microvillus, the following mass balance equations hold:

$$T^* + T = T_T \tag{1}$$

DOI 10.1007/978-1-4614-7320-6_333-1

$$CaM + C^* = C_T \tag{2}$$

$$PLC^* + PLC = PLC_T \tag{3}$$

$$G^*GDP + G + G^* + PLC^* = G_T \tag{4}$$

Using these mass balance equations, the number of state variables can be reduced and the state vector, **X**, defined as

$$\mathbf{X} = [M^*; G; G^*; PLC^*; D^*; C^*; T^*] \tag{5}$$

The details of how the state transition matrix, **V**, the number of reactant pairs, $\boldsymbol{h}$, and the stochastic reaction constant vector, $\boldsymbol{c}_{\mathbf{1}\times\mathbf{12}}$, are defined and calculated for each reaction, R1–R12, are explained in Song et al. (2012).

Calcium dynamics. Ca^{2+} is an essential feedback signal in the phototransduction cascade. Ideally, Ca^{2+} should be included as one of the state variables. However, because Ca^{2+} changes up to 1,000-fold during a bump, its dynamics is not included in the state vector (Eq. 5) but approximated by a deterministic approach (Fig. 4a) (Song et al. 2012). Otherwise, simulations via the Gillespie algorithm would become impracticably slow.

Computations can be streamlined by using hybrid techniques (Resat et al. 2001; Haseltine and Rawlings 2002; Rao and Arkin 2003; Puchalka and Kierzek 2004; Salis and Kaznessis 2005). In general, Ca^{2+} dynamics is simulated by deterministic methods as a balance between net Ca^{2+} influx, Ca^{2+} uptake by calcium buffer, and Ca^{2+} diffusion to the cell body. The net Ca^{2+} influx (pA) is the difference between Ca^{2+} influx and Ca^{2+} extrusion through Na^+/Ca^{2+} exchanger, where Ca^{2+} influx is estimated to constitute 40 % of the total ion influx. Ca^{2+} extrusion through Na^+/Ca^{2+} exchanger can be calculated from a simplified format of the Na^+/Ca^{2+} exchanger model (Luo and Rudy 1994), given that the extracellular ionic concentrations are fixed and the cell is voltage clamped. To update Ca^{2+} quantities in the stochastic simulation framework, Ca^{2+} dynamics are assumed to be so fast that the quantities can be approximated by the steady-state values. Song et al. (2012) give the formulation of this approach and explain how to update Ca^{2+} dynamics in the simulations.

Positive feedback (indicated by green dotted lines in Fig. 3): f_p is formulated as a Hill function of $[Ca^{2+}]_i$ inside a microvillus:

$$f_p\left(\left[Ca^{2+}\right]_i\right) = \frac{\left([Ca^{2+}]_i/K_P\right)^{m_p}}{1 + \left([Ca^{2+}]_i/K_P\right)^{m_p}} \tag{6}$$

where K_p is the dissociation constant, i.e., $[Ca^{2+}]_i$, that provides half occupancy of Ca^{2+} binding sites for the channels and m_p is the Hill coefficient, describing the cooperativity of Ca^{2+} in exciting the channels.

Negative feedback (indicated by red dotted arrows in Fig. 3): f_n is formulated as proportional to a Hill function of $[C^*]_i$:

$$f_n\left([C^*]_i\right) = n_s \times \frac{\left([C^*]_i/K_n\right)^{m_n}}{1 + \left([C^*]_i/K_n\right)^{m_n}} \tag{7}$$

where n_s denotes a global negative feedback strength parameter. This is one of the most important parameters in the model; it is the only parameter that is used to regulate the bump shape in our

DOI 10.1007/978-1-4614-7320-6_333-1

simulations (Fig. 7), whereas all the other kinetic parameters are fixed. K_n is the dissociation constant and m_n is the Hill coefficient for $[C^*]_i$. In reality, the affinity of $[C^*]_i$ might vary for different feedback targets, leading to different parameter values for K_n and m_n. However, for simplicity, it is assumed that the whole pool of available C^* binding sites have the same affinity properties and local feedback strengths are parameterized by h_*. This simplification provides a practical initial approximation, in the absence of more complete mechanistic knowledge concerning the different underlying processes. The related parameters (h_*, etc.) are listed in Song et al. (2012).

With the definitions of $\mathbf{V}$, $\boldsymbol{c}$, and $\boldsymbol{h}$, the time increment dt, during which the next reaction R_μ occurs, is determined as

$$dt = \frac{1}{la + a_s} \ln\left(\frac{1}{r_1}\right) \tag{8}$$

where r_1 is a uniformly distributed random number and a_s is the dot product between $\boldsymbol{c}$ and $\boldsymbol{h}(a_s = \sum_{\mu=1}^{\mu=M} c_\mu h_\mu)$. Apart from the parameter n_s in Eq. 7, la (or latency width regulator) is the only other critically important parameter in our model, affecting the latency distribution (Fig. 7). R_μ can be chosen so that Eq. 9 satisfies

$$\sum_{v=1}^{\mu-1} a_v < r_2 a_s \leq \sum_{v=1}^{\mu} a_v \tag{9}$$

where r_2 is a uniformly distributed random number and $a_v = c_v h_v$.

Simulating the phototransduction model. The stochastic bump model can accommodate complex time series of photon inputs. When a new photon input arrives, the Gillespie algorithm is stopped and the molecule numbers are updated. As described above (Fig. 4), simulations clarify why a single microvillus can only produce one bump at a time, regardless of its photon input (see above) and how bumps from a single microvillus adapt, depending on its memory state of the photon input history.

The simulated bump series can be quantified by three bump parameters, namely, bump waveform (i.e., its amplitude and duration), latency distribution, and refractory period distribution (Fig. 7). These bump parameters shape the macroscopic LIC (Juusola and Hardie 2001a, b; Song et al. 2012).

Integration of Light-Induced Current (*LIC*)

- Input: variable current bumps generated by each microvillus
- Output: macroscopic light-induced current response

Macroscopic *LIC* of the rhabdomere is integrated from the current bumps of up to 30,000 microvilli (Figs. 2 and 3).

$$LIC = \sum_{N=1}^{N=30,000} I_{in}^N \tag{10}$$

Key assumptions:

- How different microvilli cooperate in producing the *LIC* is unclear. However, it is assumed that their phototransduction cascades are independent and the macroscopic *LIC* represents the summation of bumps (Eq. 10). This assumption is valid in dim-to-medium light conditions, where experimentally obtained bump statistics indicate a one-to-one photons-to-bumps relationship (Henderson et al. 2000).

Regulating bump waveform and latency distribution statistics. Simulations can be made to match to those of recordings by single parameter adjustments. The average bump waveform can be regulated by a single "master" parameter, n_s (Eq. 7), and the average bump latency distribution by another single parameter, *la* (Eq. 8). n_s and *la* can be fixed in simulations to produce natural-like bump variations for each light-adaptation state (Figs. 6 and 7). n_s affects mostly the bump shape, whereas *la* affects mostly the bump latency (Song et al. 2012). Both of these parameters have little effect on the bump refractory period when the bump statistics were within the physiological range for *Drosophila* (Song et al. 2012).

HH Model of Photoreceptor Plasma Membrane

- Input: macroscopic light-induced current response
- Output: macroscopic light-induced voltage response

LICs can be converted to voltage responses by a Hodgkin-Huxley (*HH*) type of *Drosophila* photoreceptor cell membrane model. This incorporates voltage-gated fast inactivating Shaker and slow delayed rectifier, Shab, K^+ conductances (Hardie 1991; Hardie et al. 1991), and K^+ and Cl^- leaks. It also includes a slowly activating, non-inactivating voltage-gated K^+ conductances and the "window current" representing partial failure of Shaker channel inactivation (−11 %). The model lacks further modulation of Shab channels, which are probably located on the microvillar plasma membrane, via phosphoinositide depletion (Krause et al. 2008) and the fast delayed rectifier (Shal current). The conductance for Cl^- leak can be used to regulate the resting potential (Niven et al. 2003; Vähäsöyrinki et al. 2006). The light-dependent conductance is not included, because the phototransduction cascade model provides the functional equivalence to this conductance.

Global feedback mechanisms. To replicate the effect of slow global feedbacks, such as intracellular accumulation or diffusion of Ca^{2+}, a global feedback strength parameter can be implemented in the phototransduction cascade model (n_s in Eq. 7). In the simplest case, by changing n_s exponentially (Eq. 11), the model reproduces the slow light-adaptation trends (exponential decay to plateau) in the *LIC* responses to light pulses (Fig. 5):

$$n_s = n_{s0} + A_{n_s} - A_{n_s}\exp(-t/\tau_{n_s}) \tag{11}$$

where n_{s0} denotes the initial condition for n_s, $n_{s0} + A_{n_s}$ is the value for n_s at, t_∞ and τ_{n_s} is the time constant of n_s dynamics. These parameters for n_s at different light levels can be found in Song et al. (2012).

Owing to the model structure, the voltage regulation of the TRP/TRPL channels' driving force can be implemented as a global feedback mechanism. This procedure reveals the interplay between the light-sensitive and light-insensitive membrane, when the photoreceptor is encoding vast changes in light intensity.

Specifically, I_{in}, formulation from Eqs. 1 to 12 can be modified:

DOI 10.1007/978-1-4614-7320-6_333-1

$$I_{in}^{N} = (T^{*}N)(g_{TRP})(TRP_{rev} - V_m) \tag{12}$$

where T^{*N} is the number of opened TRP/TRPL channels in the *Nth* microvillus, g_{TRP} is the single TRP channel conductance, TRP_{rev} is TRP channel reversal potential, and V_m is the membrane voltage. g_{TRP} can be formulated according to Eq. 13:

$$g_{TRP} = 8 \times \begin{cases} 1 & \text{if} \quad TRP_{rev} > V_m \\ 0 & \text{otherwise} \end{cases} \tag{13}$$

In this way, TRP/TRPL channels are either fully closed or fully opened, with a single-channel conductance of 8 pS in the open state. TRP_{rev} is set to 0 mV (Hardie and Postma 2008).

From Eq. 12, as membrane voltage (V_m) increases, the bumps (I_{in}^{N}) shrinks accordingly, reducing the overall macroscopic *LIC* response (Eq. 10). Since the phototransduction cascades and the membrane are modeled separately in two compartments, the cell membrane voltage (V_m) is obtained by injecting *LIC* into the Hodgkin-Huxley-type cell body model

$$V_m = HH(LIC) \tag{14}$$

where *HH* is a function representing the cell membrane model.

The iteration process is conducted between these two model compartments (Eqs. 10, 11, 12, and 13) to obtain realistic macroscopic *LIC*s and voltage responses. Thus, the calculation of I_{in}^{N} in Eq. 12 requires membrane potential feedback, V_m, which is initialized at the resting potential (−70 mV). As a result, I_{in}^{N} in every microvillus is larger than the true value, and hence LIC_0 obtained in Eq. 10 is larger than the true value of *LIC*. Accordingly, LIC_0 charges a too large voltage response V_{m1}. To obtain a more realistic *LIC*, V_{m1} is fed back to Eq. 12; but as a result, LIC_1 can be smaller than the true value (i.e., the obtained values oscillate). Hence, an iterative simulation procedure between rhabdomere and the cell body is conducted to acquire the converged *LIC* and V_m. Here, it is assumed that the voltage feedback only affects the amount of current influx through the opened TRP/TRPL channels but not the dynamics of the phototransduction; T^{*N} is not changing in each microvillus.

References

Dippe MAZ, Wold EH (1985) Antialiasing through stochastic sampling. Comput Graph 19:69–78

Fain GL, Hardie R, Laughlin SB (2010) Phototransduction and the evolution of photoreceptors. Curr Biol 20:R114–R124

Faivre O, Juusola M (2008) Visual coding in locust photoreceptors. PLoS One 3:e2173

Galton F (1907) Vox populi. Nature 75:450–451

Gillespie DT (1976) General method for numerically simulating stochastic time evolution of coupled chemical-reactions. J Comput Phys 22:403–434

Gonzalez-Bellido PT, Wardill TJ, Juusola M (2011) Compound eyes and retinal information processing in miniature dipteran species match their specific ecological demands. Proc Natl Acad Sci USA 108:4224–4229

Hardie RC (1991) Voltage-sensitive potassium channels in *Drosophila* photoreceptors. J Neurosci 11:3079–3095

Hardie RC (1996) INDO-1 measurements of absolute resting and light-induced Ca2+ concentration in *Drosophila* photoreceptors. J Neurosci 16:2924–2933

Hardie RC (2012) Phototransduction mechanisms in *Drosophila* microvillar photoreceptors. WIRES Membr Transp Signal 2011:2162–2187

Hardie RC, Postma M (2008) Phototransduction in microvillar photoreceptors of *Drosophila* and other invertebrates. In: Basbaum AI, Kaneko A, Shepherd GM, Westheimer G (eds) The senses: a comprehensive reference. Vision. Academic, San Diego, pp 77–130

Hardie RC, Franze K (2012) Photomechanical responses in *Drosophila* photoreceptors. Science 338:260–263

Hardie RC, Voss D, Pongs O, Laughlin SB (1991) Novel potassium channels encoded by the Shaker locus in *Drosophila* photoreceptors. Neuron 6:477–486

Haseltine EL, Rawlings JB (2002) Approximate simulation of coupled fast and slow reactions for stochastic chemical kinetics. J Chem Phys 117:6959–6969

Heimonen K, Salmela I, Kontiokari P, Weckström M (2006) Large functional variability in cockroach photoreceptors: optimization to low light levels. J Neurosci 26:13454–13462

Henderson SR, Reuss H, Hardie RC (2000) Single photon responses in *Drosophila* photoreceptors and their regulation by Ca2+. J Physiol 524(Pt 1):179–194

Hochstrate P, Hamdorf K (1990) Microvillar components of light adaptation in blowflies. J Gen Physiol 95:891–910

Howard J, Blakeslee B, Laughlin SB (1987) The intracellular pupil mechanism and photoreceptor signal: noise ratios in the fly *Lucilia cuprina*. Proc R Soc Lond B Biol Sci 231:415–435

Huang J, Liu CH, Hughes SA, Postma M, Schwiening CJ, Hardie RC (2010) Activation of TRP channels by protons and phosphoinositide depletion in *Drosophila* photoreceptors. Curr Biol 20:189–197

Juusola M, Weckstrom M (1993) Band-pass filtering by voltage-dependent membrane in an insect photoreceptor. Neurosci Lett 154:84–88

Juusola M, Hardie RC (2001a) Light adaptation in *Drosophila* photoreceptors: I. Response dynamics and signaling efficiency at 25 degrees C. J Gen Physiol 117:3–25

Juusola M, Hardie RC (2001b) Light adaptation in *Drosophila* photoreceptors: II. Rising temperature increases the bandwidth of reliable signaling. J Gen Physiol 117:27–42

Juusola M, de Polavieja GG (2003) The rate of information transfer of naturalistic stimulation by graded potentials. J Gen Physiol 122:191–206

Krause Y, Krause S, Huang J, Liu CH, Hardie RC, Weckstrom M (2008) Light-dependent modulation of Shab channels via phosphoinositide depletion in *Drosophila* photoreceptors. Neuron 59:596–607

Laughlin SB, de Ruyter van Steveninck RR, Anderson JC (1998) The metabolic cost of neural information. Nat Neurosci 1:36–41

Leneman OAZ (1966) Random sampling of random processes: impulse response. Info Control 9:347–363

Liu CH, Satoh AK, Postma M, Huang J, Ready DF, Hardie RC (2008) Ca2 + -dependent metarhodopsin inactivation mediated by calmodulin and NINAC myosin III. Neuron 59:778–789

Luo CH, Rudy Y (1994) A dynamic model of the cardiac ventricular action potential. I. Simulations of ionic currents and concentration changes. Circ Res 74:1071–1096

Mishra P, Socolich M, Wall MA, Graves J, Wang Z, Ranganathan R (2007) Dynamic scaffolding in a G protein-coupled signaling system. Cell 131:80–92

Niven JE, Vahasoyrinki M, Kauranen M, Hardie RC, Juusola M, Weckstrom M (2003) The contribution of Shaker K + channels to the information capacity of *Drosophila* photoreceptors. Nature 421:630–634

Padmanabhan K, Urban NN (2010) Intrinsic biophysical diversity decorrelates neuronal firing while increasing information content. Nat Neurosci 13:1276–1282

Postma M, Oberwinkler J, Stavenga DG (1999) Does Ca2+ reach millimolar concentrations after single photon absorption in *Drosophila* photoreceptor microvilli? Biophys J 77:1811–1823

Puchalka J, Kierzek AM (2004) Bridging the gap between stochastic and deterministic regimes in the kinetic simulations of the biochemical reaction networks. Biophys J 86:1357–1372

Pumir A, Graves J, Ranganathan R, Shraiman BI (2008) Systems analysis of the single photon response in invertebrate photoreceptors. Proc Natl Acad Sci USA 105:10354–10359

Rao CV, Arkin AP (2003) Stochastic chemical kinetics and the quasi-steady-state assumption: application to the Gillespie algorithm. J Chem Phys 118:4999–5010

Resat H, Wiley HS, Dixon DA (2001) Probability-weighted dynamic Monte Carlo method for reaction kinetics simulations. J Phys Chem B 105:11026–11034

Salis H, Kaznessis YN (2005) An equation-free probabilistic steady-state approximation: dynamic application to the stochastic simulation of biochemical reaction networks. J Chem Phys 123

Scott K, Sun Y, Beckingham K, Zuker CS (1997) Calmodulin regulation of *Drosophila* light-activated channels and receptor function mediates termination of the light response in vivo. Cell 91:375–383

Shannon CE (1948) A mathematical theory of communication. Bell Syst Technical J 27:379–423

Song Z, Postma M, Billings SA, Coca D, Hardie RC, Juusola M (2012) Stochastic, adaptive sampling of information by microvilli in fly photoreceptors. Curr Biol 22:1371–1380

Vähäsöyrinki M, Niven JE, Hardie RC, Weckström M, Juusola M (2006) Robustness of neural coding in *Drosophila* photoreceptors in the absence of slow delayed rectifier K + channels. J Neurosci 26:2652–2660

Wardill TJ, List O, Li X, Dongre S, McCulloch M, Ting CY, O'Kane CJ, Tang S, Lee CH, Hardie RC, Juusola M (2012) Multiple spectral inputs improve motion discrimination in the *Drosophila* visual system. Science 336:925–931

Wong F, Knight BW (1980) Adapting-bump model for eccentric cells of limulus. J Gen Physiol 76:539–557

Wong F, Knight BW, Dodge FA (1980) Dispersion of latencies in photoreceptors of *Limulus* and the adapting-bump model. J Gen Physiol 76:517–537

Wong F, Knight BW, Dodge FA (1982) Adapting bump model for ventral photoreceptors of *Limulus*. J Gen Physiol 79:1089–1113

Yau KW, Hardie RC (2009) Phototransduction motifs and variations. Cell 139:246–264

Yellott JI Jr (1982) Spectral analysis of spatial sampling by photoreceptors: topological disorder prevents aliasing. Vision Res 22:1205–1210

Zheng L, de Polavieja GG, Wolfram V, Asyali MH, Hardie RC, Juusola M (2006) Feedback network controls photoreceptor output at the layer of first visual synapses in *Drosophila*. J Gen Physiol 127:495–510

Zheng L, Nikolaev A, Wardill TJ, O'Kane CJ, de Polavieja GG, Juusola M (2009) Network adaptation improves temporal representation of naturalistic stimuli in *Drosophila* eye: I dynamics. PLoS One 4:e4307